Enhanced Selectivity and Stability of Ruthenium Purple-Modified Carbon Fiber Microelectrodes for Detection of Hydrogen Peroxide in Brain Tissue

Ana Ledo[1,2], Eliana Fernandes[1], Christopher M.A. Brett[3], Rui M. Barbosa[1,2]

[1] University of Coimbra, Faculty of Pharmacy, Azinhaga de Santa Comba, 3004-548 Coimbra, Portugal

[2] Center for Neuroscience and Cell Biology, University of Coimbra, Faculty of Medicine, Rua Larga, 3004-504 Coimbra, Portugal

[3] University of Coimbra, Department of Chemistry, Faculty of Sciences and Technology, 3004-535 Coimbra, Portugal

[&]Corresponding Author

Rui M. Barbosa

rbarbosa@ff.uc.pt

Faculty of Pharmacy, University of Coimbra

Azinhaga de Santa Comba

3004-548 Coimbra, Portugal

Abstract

Microelectrodes coupled to fast electrochemical techniques are an attractive approach towards real time *in vivo* monitoring with minimal damage to living tissue. Here, carbon fiber microelectrodes (CFM) were modified by electrodeposition of ruthenium purple (RP) for monitoring of H_2O_2 concentration dynamics in brain tissue preparations. The RP-modified CFM (CFM-RP) showed catalytic activity for the reduction of H_2O_2 at -0.1 V vs. Ag/AgCl in aqueous electrolyte at neutral pH and in the presence of physiological concentration of sodium cation (154 mM). The CFM-RP displayed a linear response in the concentration range of 2-500 µM, with a sensitivity of 0.98 ± 0.37 µA cm^{-2} μM^{-1} and a limit of detection of 70 ± 40 nM. Coating the CFM-RP with a Nafion® layer greatly extended the operational stability of the RP film to 3 hours in a medium containing a high sodium concentration at physiological pH 7.4. Validation of the CFM-RP-Nafion® sensor suitability for monitoring H_2O_2 concentration dynamics was achieved by measuring exogenously and locally applied H_2O_2 in rodent striatal slices. Together, these results support the excellent analytical performance of this new CFM-RP-Nafion® sensor design for sensitive and selective monitoring of H_2O_2 concentration dynamics in brain tissue.

Keywords: Carbon fiber microelectrode; ruthenium purple; hydrogen peroxide; brain slices.

1. Introduction

Hydrogen peroxide (H_2O_2) is a membrane-permeable messenger and biological oxidant which acts as an intercellular and intracellular signaling molecule. Although it was considered for a long time as a toxic cellular waste resulting from oxidative metabolism, accumulating evidence has come to show that this and other oxidants such as superoxide are important and normal components of signaling pathways [1]. In the brain, H_2O_2 regulates neuronal activity and growth, neuron-glia and neuron-neuron signaling, including neurotransmission and plasticity [2]. Thus, the ability to monitor dynamic changes in H_2O_2 concentration is essential for our understanding of its bioactivity in brain tissue.

Microelectrodes coupled to fast electrochemical techniques are an attractive approach towards H_2O_2 monitoring in brain tissue. Due to its facile oxidation on platinum surfaces, some authors have used direct electro-oxidation of H_2O_2 using amperometry. However, the relatively high positive potential (>+0.6V vs. Ag/AgCl) required for H_2O_2 oxidation and the presence of many oxidizable substances in biological media (ascorbate, amines, etc.) can lead to non-specific interferences. This imposes the need to use permselective membranes to guarantee selectivity, with a compromise in performance towards H_2O_2 detection [3–6]. Others have explored fast cyclic voltammetry (FCV) to achieve selectivity as a result of the molecular fingerprinting this approach affords [7,8]. A caveat related with this approach is the requirement for signaling processing and background subtraction. Others have designed a dual amperometric H_2O_2 biosensor consisting of H_2O_2 detection (blank) and degradation (catalase-immobilized) electrode arrays [9].

An alternative solution has been to use electron mediators as electrochemical transducers such as Prussian Blue (PB), introduced in the 1990's by Karyakin et al. as a platform for the design of oxidase-based biosensors [10,11]. The structure and electrochemical properties of PB, a ferric hexacyanoferrate coordination compound known as an "artificial enzyme peroxidase", has been extensively reviewed in [12]. Its most attractive property is that it allows the electrocatalytic reduction of H_2O_2 at an applied potential close to 0.0 V vs. SCE, thus minimizing the interference of reductants such as ascorbate and biogenic amines [13]. Despite its interesting properties, PB shows

poor stability at physiological pH and in the presence of the high Na^+ concentrations that occur in relevant biological settings [14]. At neutral or alkaline pH, the strong interaction of OH^- with Fe^{3+} forms $Fe(OH)_3$ [15]. Moreover, cations such as K^+, NH_4^+, Cs^+ and Rb^+ whose hydrated ionic radius fits the PB lattice are able to promote the electrochemical activity of PB; however, Na^+ and other cations have larger hydrated radii and do not support the PB redox cycle [16,17].

Other polynuclear transition metal hexacyanoferrates (MHCFs), that are PB analogues, such as nickel, cobalt, palladium, manganese, vanadium and ruthenium hexacyanoferrates have been also used as electron mediators, exhibiting good electrocatalytic activity towards H_2O_2 reduction [17–19]. In addition, they are more stable in neutral or alkaline buffer solutions and their electrochemical behavior is less affected by the presence of the dominant cations present in biological media such as Na^+, H^+, Ca^{2+} and Mg^{2+}.

Ruthenium hexacyanoferrate, also known as ruthenium purple (RP) [20], has been explored for the design of glucose oxidase-based biosensors on an Au-electrode support [21]. However, the use of thin-film RP microelectrodes based on low-cost carbon fiber microelectrodes (CFM) for monitoring extracellular H_2O_2 fluctuations in brain tissue has not, to the best of our knowledge, been investigated.

Here, we have explored the artificial peroxidase properties of RP to develop a thin film modified carbon fiber microelectrode capable of measuring rapid changes of H_2O_2 in brain slices with high sensitivity and selectivity. Furthermore, we have used a Nafion® coating to improve the operational stability of the RP thin film under conditions of constant applied potential.

2. Materials and Methods

2.1. Chemicals and Reagents

All chemicals were of analytical grade, were used as received and were obtained from Merck. Argon was provided by Air Liquide, Portugal and Carbox (95% $_{O2}$/5%CO_2) was obtain from Linde Sogas, Portugal. All solutions were prepared in ultra-pure deionized water (≥18 MΩ cm) from a Milli-Q system (Millipore Company, Bedford, MA, USA). The electrolyte solution used to evaluate the general electroanalytical properties of CFM-RP was 0.1 M KCl with 0.01 M HCl, pH 2.0. The buffer solution used for measurement of microelectrode responses was 0.01 M phosphate-buffered saline (PBS), pH 7.4 containing (in mM): 8.1 Na_2HPO_4, 1.8 KH_2PO_4, 137 NaCl and 2.7 KCl. The working solution of 9.8 mM hydrogen peroxide, and 20 mM ascorbic acid were prepared freshly each day. Stock solutions of dopamine, DOPAC, 5-hydroxytryptamine and norepinephrine were prepared in 70% perchloric acid at a concentration of 5mM.

2.2. Animals

All the procedures used in this study were performed in accordance with the European Union Council Directive for the Care and Use of Laboratory animals, 2010/63/EU, and were approved by the local ethics committee (ORBEA) and the Portuguese Directorate-General for Food and Veterinary. One male Wistar rat weighing 300 g (Charles-River Laboratories, Barcelona, Spain) was used in these experiments. While in the animal facility, animal husbandry conditions were as follows: housed in pairs in filter-topped type III Makrolon cages in the local vivarium with controlled environmental conditions, namely a temperature of 22−24°C, relative humidity of 45−65%, air exchange rate of 15 times per hour, 12 h light/dark cycle, and with standard rat chow diet (4RF21-GLP Mucedola, SRL, Settimo Milanese, Italy) and chlorinated water available *ad libitum*.

2.3. Carbon Fiber Microelectrode Fabrication

Carbon fiber microelectrodes (CFM) were fabricated as previously described [22]. Briefly, a single carbon fiber (30 µm o.d.; Textron Lowell, MA, USA) was inserted into a borosilicate glass capillary (1.16 mm i.d. and 2.0 mm o.d.; Harvard Apparatus, Holliston, MA, USA) and cleaned with acetone. Each capillary was pulled on a vertical puller (Harvard Apparatus, UK) and the protruding carbon fiber was cut to a tip length of

approx. 150 µm. The electrical contact between the carbon fiber and the copper wire was provided by conductive silver paint (RS, Northants, UK). The microelectrodes were tested for general recording properties in 0.05 M PBS Lite (in mM: 10 Na_2HPO_4, 40 NaH_2PO_4, and 100 NaCl, pH 7.4) by fast cyclic voltammetry at a scan rate of 200 V s^{-1}, between -0.4 and +1.6 V vs. Ag/AgCl for 30 cycles).

2.4. Modification of CFM Surface with Ruthenium Purple

Following the procedure described in [23], the RP solution for electrodeposition onto the CFM surface was prepared freshly on the day of experiment and used within 4 hours. A solution of 1mM $K_4[Ru^{II}(CN)_6]$ prepared in 35mM KCl (N_2-purged) was mixed, under vigorous stirring, with a solution of 1mM $FeCl_3$ / 35 mM KCl (N_2-purged). Special care should be taken to guarantee that the ionic strength does not exceed 40 mM and that the molar ratio $FeCl_3$ / $K_4[Ru^{II}(CN)_6]$ is <1 [24]. The pH of the resulting colloidal suspension was adjusted to 2.0 using 1 M HCl. This solution was placed in an ultrasound bath and $RuCl_3$ was added from a 1 mM solution to give a final concentration of 20 µM.

To prepare a thin film of RP on the CFM surface, electrodeposition was carried out by potential cycling between -0.2 and +1.0 V vs. Ag/AgCl at a scan rate of 50 mV s^{-1}. The cycles were repeated until the peaks no longer increased in height. The modified CFM was rinsed with distilled water and placed in a solution of 1 mM $RuCl_3$ / 35 mM KCl. Between 2 and 4 further cycles were performed under the same conditions to ensure the stability of the deposited film. For coating with Nafion®, the tip of the CFMs modified with RP (CFM-RP) were dipped into a 5% solution of Nafion® in aliphatic alcohols for 5 s and then dried at 100 ºC for 15 min. These sensors were designated CFM-RP-Nafion®.

2.5. Scanning electron microscopy

High-resolution scanning electron microscopy (SEM) was performed using a field emission scanning electron microscope coupled with energy dispersive X-ray spectroscopy (EDS) (Zeiss Merlin coupled to a GEMINI II column). The elemental composition was obtained from backscattered electron detection using EDS at 10 keV (Oxford Instruments X-Max). Conductive carbon adhesive tabs were used to ground the exposed copper wire at the end of the CFM and secure the sample on the specimen holder.

2.6. Preparation of Rat Striatam Slices

Following decapitation under deep anesthesia (isoflurane), the brain of the animal was rapidly removed and placed in ice-cold, Carbox bubbled isolation aCSF with the following composition (in mM): 124 NaCl, 4.5 KCl, 2 $CaCl_2$, 1 $MgCl_2$, 26 $NaHCO_3$, 1.2 NaH_2PO_4, 1 glutathione, 0.2 ascorbic acid and 10 D-glucose. The cerebellum was removed, the two hemispheres were separated and mounted in the pre-chilled stage of a vibratome (Vibroslice, World Precision Instruments) and submerged in the chamber filled with ice cold isolation aCSF continuously bubbled with Carbox. This medium should be chilled to the point that ice chips are present. Brain slices containing the striatum were obtained with a thickness of 400 µm and transferred to a pre-incubation chamber (BSC-PC; Harvard Apparatus) filled with isolation aCSF. Slices were allowed to recover under these conditions for at least 1 h prior to recording.

2.7. Recording H_2O_2 in Rat Striatal Slices

In order to record H_2O_2 in striatal slices, an individual slice was place in a recording chamber (BSC-BU with BSC-ZT top, Harvard Apparatus) and perfused with aCSF with the following composition (in mM): 124 NaCl, 4.5 KCl, 2 $CaCl_2$, 1 $MgCl_2$, 26 $NaHCO_3$, 1.2 NaH_2PO_4, and 10 D-glucose which was continuously bubbled with humidified Carbox. The temperature of the chamber was maintained at 32 °C (temperature controller model TC-202A, Harvard Apparatus) and the flow rate was fixed at 2 ml/min. A recording array comprised of a CFM-RP-Nafion® and a CFM mounted at a tip-to-tip distance of 100 µm was lowered into the tissue with the aid of a micromanipulator so as to guarantee that the totality of the active surface was in the tissue core. Recording of the cathodic current was initiated and once a stable baseline was obtained, an H_2O_2 solution (1mM in aCSF) was pressure ejected via a Picospritzer II (General Valve, Fairfield, NJ). Through a pulled micropipette, placed between the two working electrodes. A schematic representation of the setup for electrochemical recording in striatal slices is shown in Fig. S1.

2.8. Electrochemical Instrumentation

All *in vitro* electrochemical procedures were performed using a Multi PalmSens4 Potentiostat (PalmSens, The Netherlands) controlled by MultiTrace v.4.2 software

(PalmSens, The Netherlands). For all procedures, a 3-electrode electrochemical cell was used, comprised of the working electrode, an Ag/AgCl in 3 M NaCl reference electrode (RE-5B, BAS Inc., IN, USA), and a Pt wire as auxiliary electrode.

Amperometric recording in slices and calibration in the slice recording chamber were performed using a FAST16mkII potentiostat (Quanteon, KY, USA) in a 2-elecrtode electrochemical cell configuration comprised of the working electrode and an Ag/AgCl pellet reference electrode.

2.9. Data Analysis

Data analysis was performed using MultiTrace v. 2.6, FAST Analysis version 6.0, OriginPro 2016, and GraphPad 5.0. Values are given as the mean ± SD. The number of repetitions is indicated in each individual determination. The sensitivity of CFM-RP toward H_2O_2 reduction was determined by linear regression analysis in the range of 0−10 µM. The limit of detection (LOD) was defined as the concentration that corresponds to a signal-to-noise ratio of 3, considering the following expression:

$$LOD = \frac{3\,SD}{m}$$

where SD represents the standard deviation of the baseline and *m* is the slope of the respective calibration curve [25].

3. Results and Discussion

3.1. Determination of the EAS of the CFMs.

A standard electrochemical redox couple was used to determine the electrochemical behavior of the CFMs and determine the electrochemically active surface area. Cyclic voltammetry was carried out in 5.0 mM hexammineruthenium(III) chloride ($Ru^{III}(NH_3)_6$) in 0.5 M KCl solution at scan rates from 25 to 200 mV s^{-1}. As can be observed in Figure S2A, the CVs revealed a well-defined symmetrical redox pair appearing at v > 25 mV s^{-1}. Both anodic and cathodic peak currents ($I_{p,a}$ and $I_{p,c}$, respectively) varied linearly with the square root of the scan rate (Figure S2B; R^2 values of 0.999, for $I_{p,a}$ and $I_{p,c}$) indicating that the process was diffusion-controlled. The average $I_{p,a}$ / $I_{p,c}$ ratio at 25 mV s^{-1} was 0.97 +/- 0.03 (n = 8), which is close to the theoretical value of 1 for a totally reversible reaction.

The electrochemically active surface area of the CFMs was estimated using the Randles-Sevick equation for a reversible oxidation−reduction reaction considering a diffusion coefficient of $D = 9.1 \times 10^{-6}$ cm^2 s^{-1} [26]. The calculated surface area of the bare CFMs was found to be 1.61 x 10^{-4} ± 0.79 x10^{-4} cm^2 (N=76), ranging between 3.12 x 10^{-5} and 5.54 x 10^{-4} cm^2, reflecting the different tip lengths.

3.2. Electrodeposition of RP in CFM surface

The electrodeposition of RP onto the surface of CFM was carried out from a mixture of Fe^{3+} and $Ru^{II}(CN)_6^{4-}$ by potential cycling between -0.2 and +1.0 V vs. Ag/AgCl at a scan rate of 50 mV s^{-1}. As can be observed in Fig. 1A, this procedure resulted in a gradual electrodeposition of the RP film with increase in both anodic and cathodic peak currents. Typically, 10 to 15 cycles were performed, until no increase in peak currents was observed. Further cycling decreased the peak currents, indicating saturated coverage of the carbon surface and thicker films leading to electrical resistance effects. Following RP electrodeposition, the CFM was placed in 1 mM $RuCl_3$ / 35 mM KCl solution and an additional four scans were performed under the same conditions. This completed the fabrication of RP-modified CFMs (CFM-RP).

The RP-modified CFM (CFM-RP) was characterized by cyclic voltammetry. A representative cyclic voltammogram for a CFM-RP in KCl (0.1M) + HCl (0.01 M) solution

at 50 mV s^{-1} is shown in Fig. S3. As previously reported, the electrodeposited RP has a single redox couple attributed to the following reaction [24,27,28]:

$$\underset{\text{Ruthenium Purple (RP)}}{Fe_4^{III}[Ru^{II}(CN)_6]_3} + 4K^+ + 4e^- \rightarrow \underset{\text{Ruthenium White (RW)}}{K_4Fe_4^{II}[Ru^{II}(CN)_6]_3}$$

The mean value of $E_{1/2}$ = ($E_{p,a}$+$E_{p,c}$)/2 was 173.4 ± 4.0 mV (N=6), in agreement with previously reported values for RP films electrodeposited under similar conditions on glassy carbon (GC) (155-180 mV [24,29]), Au (180 mV, [29], Pt (172 mV, [28]) and indium tin oxide (ITO) (185 mV, [30]. Furthermore, at a scan rate of 50 mV s^{-1}, the mean peak-to-peak separation, ΔE_p, was 43.7 ± 2.9 mV (N=6).

In biological media, and in the brain in particular, sodium ion is the predominant cation and the pH typically ranges between 7.2 in the intracellular compartment and 7.4 in the extracellular space [31]. Thus, the RP film was also characterized by cyclic voltammetry in 10 mM phosphate buffer, pH 7.4 with varying K^+/Na^+ ratios (total [cation] of 158 mM). As shown in Fig. 1B, in a buffer containing only K^+, the 2 typical cathodic waves ($I_{c(I)}$ and $I_{c(II)}$) and single anodic wave (I_a) were observed. As the K^+/Na^+ ratio decreased, a significant decrease in both cathodic and anodic peak currents was observed as well as a negative shift in both reduction and oxidation potentials. This shift results from the different affinity of the RP film towards the cation (K^+>Na^+) due to the different size of the hydrated cation (Na^+>K^+) which impacts its ability to enter the crystal lattice during the electrochemical reduction process without deforming it [16,17].

3.3. Surface Properties: Morphology, Coverage and Film Thickness

The morphology of the CFM-RP surface was examined by SEM and, as seen in Fig. 2, the electrodeposition procedure employed here resulted in the full coverage of the carbon surface of the CFM with cubes and agglomerates of RP. The energy dispersive X-ray spectrogram in Fig. 2D confirms the presence of Fe and Ru on the CFM-RP surface, not seen on the bare CFM surface (not shown).

Cyclic voltammetry of the RP film deposited on the CFM was done at scan rates in the range 0.01 – 5 V s^{-1} in 0.1 M KCl / 0.01 M HCl (Fig. 3A). Both anodic and cathodic peak currents showed a linear dependence on scan rate for ν < 0.3 V s^{-1} (Fig. 3B), indicative of a surface-confined process that can be associated with charge movement in the RP film. The relationship between peak current (I_p) and scan rate (ν) is [32]:

$$I_p = \frac{n^2 F^2 A \Gamma \nu}{4RT}$$

where Γ and A represent, respectively, the surface concentration and the electrochemical active surface area and R, F and T have their usual meanings. From this expression and using the slope obtained from the $I_{p,a}$ vs. ν plots, the average RP surface concentration at the CFM surface was calculated as **2.48± 0.71 x 10^{-9} mol cm^{-2} (n=10)**. This is higher than that reported for RP films electrodeposited on gold microelectrodes (3.34 x10^{-10} mol cm^{-2} [21]) as well as on clay modified electrodes (5 x 10^{-11} mol cm^{-2}, [33], but lower than values reported for GC (8.5 x 10^{-9} mol cm^{-2} [34]) and ITO electrodes (2.8 x 10^{-8} mol cm^{-2} [30]).

The thickness of the RP film, l, was estimated considering the number of unit cells present, geometrical parameters of the RP cell and the electrochemical surface area, according to the following expression [35]:

$$l = \Gamma \frac{a^3 N_A}{4}$$

where N_A is Avogadro's number and a represents the unit cell parameter, which is 1.042 nm for RP [28] . The thickness of the RP film was thus calculated to be **4.23 ± 1.2 nm (n=10).**

For scan rates above 0.3 V s^{-1}, both cathodic and anodic peak currents varied linearly with the square root of scan rate ($\nu^{1/2}$), indicating a diffusion-controlled process due to insertion/expulsion of chemical species in solution, namely K^+ . Fig. 3A also shows

that the peak separation increases at higher scan rates, a result of limiting charge transfer kinetics. Plotting ($E_p - E^{o\prime}$) as a function of log (ν) (Fig. 3D) revealed a linear dependence at high scan rates. Kinetic parameters, namely the surface electron transfer rate constant (k_s) and the anodic charge transfer coefficient (α_a) can be estimated by using the following equation derived by Laviron for $n\Delta E_p > 200$ mV [36,37]:

$$E_{ox} = E^{o\prime} + \left[\frac{RT}{\alpha_a nF}\right] ln\left\{\left[\frac{\alpha_a nF}{2.303RT}\right]\left[\frac{\upsilon}{k_s}\right]\right\}$$

From the linear fitting of the plot E_{ox} vs. log n in Fig. 3D for high scan rates:

$$Slope = S_a = \frac{2.303RT}{\alpha_a nF}$$

and

$$Intercept = E^{o\prime} + S_a\, log\left(\frac{2.303}{S_a}\right) - S_a \log(k_s)$$

where $E^{o\prime}$ was considered as $E_{1/2}$ for a scan rate of 0.010 V s^{-1}. The values of α_a and k_s were 0.24 ± 0.02 and 1.73 ± 0.08 s^{-1} (n=5), respectively. The electron transfer rate constant is in good agreement with that reported previously for RP-films (Shen-Ming 2003). The α_a value below 0.5 means that the redox transition state is not symmetrical and more on the side of the reduced state.

3.4. Operational Stability

One of the major advantages of RP over PB thin films is the increased operational stability of the film in physiological pH and in the presence of a high concentration of Na^+ (ca. 150 mM) and low concentration of K^+ (ca. 4 mM), as observed in biological media. The stability of the RP film was evaluated by performing 100 cyclic voltammograms at a scan rate of 50 mV s^{-1} in two electrolytes of different ion composition and pH. As can be seen in Fig. 4A, the $I_{p,c(n)}/I_{p,c(1)}$ ratio, calculated using

cathodic peak current for each cycle ($I_{p,c(n)}$) and normalizing for the first one ($I_{p,c(1)}$), remained stable, highlighting the good operational stability of the RP film in both conditions.

To explore the stability of the RP film in PBS pH 7.4, CVs were repeated during 3.5 hours (Fig. 4B). The purple symbols show the $I_{p,c(n)}/I_{p,c(1)}$ of the CFM-RP and reveal that the RP film remains stable on the surface of the CFM for the whole period under these conditions. To understand the operational stability of the RP film under constant recording conditions, the potential was held at -0.1 V vs. Ag/AgCl between successive CV scans. As shown in the black trace in Fig. 4B, the RP film remains stable for up to 20 min and then begins to degrade. For comparative purposes, the same evaluation was performed for a CFM modified by electrodeposition of Prussian blue (CFM-PB) and, as expected, a poor stability is observed [38]. These results suggest that the degradation of the RP film is a result not of pH or the presence of a high Na^+ concentration in the medium, but rather the maintenance of the crystal in the reduced, ruthenium white, state.

In the case of PB films, addition of surfactants during electrodeposition has been shown to increase operational stability of the crystal [35,39]. Carbon nanotubes have also been reported to improve the stability of both PB and RP-based electrodes [40–42]. We explored the ability of Nafion® to increase the operational stability of CFM-RP. For this purpose, the tip of the CFM-RP was coated with Nafion® by dipping into a 5% Nafion® solution in aliphatic alcohol, followed by drying at 100 ºC for 15 min. A small decrease of the $I_{p,c(n)}/I_{p,c(1)}$ = 0.80, was observed after 3 hours (Fig 3B red symbol trace) indicating that this permselective film significantly enhances RP film stability in PBS at pH 7.4. Nafion® membranes are well known proton-conductive polymer films and their stabilizing ability has been shown for PB, where it was hypothesized that Nafion® alters the exchange between Fe^{3+} and K^+ during conversion of the insoluble (K^+-free) and soluble ($KFe[Fe(CN)_6]$-bound) forms of PB [43].

3.5. Electroanalytical Properties Towards H_2O_2

Similar to Prussian white (the reduced form of PB), ruthenium white has also been reported to catalytically reduce H_2O_2 [21], making it an attractive support for monitoring this biological oxidant. The electrocatalytic activity of the CFM-RP towards H_2O_2 was

assessed in PBS solution containing 4.5 mM K^+ at pH 7.4 by linear sweep voltammetry at 50 mV s^{-1}. As can be observed in Fig. 5A, the presence of increasing the concentration of H_2O_2 from 100 to 300 µM resulted in a proportional increase in the cathodic response in the range of +0.1 V to -0.4 V vs. Ag/AgCl. A similar profile was observed for the CFM-RP-Nafion®, although a decrease in peak current was observed (Fig. 5B). This decrease has been previously reported and results from the increased resistance of counterion transport through the electroactive film [43].

To determine the optimal applied potential for H_2O_2 monitoring in the presence of ascorbate and O_2 in biological media using constant potential amperometry, the amperometric response for each analyte was recorded at applied potentials in the range between -0.2 and +0.2 V vs. Ag/AgCl for CFM-RP and CFM-RP-Nafion®. As shown in the black trace of Fig. 5C, the mean sensitivity towards H_2O_2 of the CFM-RP sensor increased from +0.2 to -0.2 V while the oxidation current for ascorbate increased for applied potentials above 0 V, the reduction current for O_2 being detected only for an applied potential less than -0.05 V. Coating with Nafion® decreased the sensitivity towards H_2O_2 61% at E = -0.05 V and 21% at E = -0.2V, and oxidation of ascorbate was detectable above -0.05 V while the reduction of O_2 remained undetectable within the potential window analyzed (Fig. 5D). The selectivity ratios calculated for each applied potential are summarized in Fig. S4A.

From these results and considering the extracellular concentration of ascorbate and O_2 expected *in vivo* in the brain extracellular space of ca. 500 µM and 30 µM , respectively [44–46], an optimal applied potential of -0.1 V vs. Ag/AgCl was selected for amperometric detection of H_2O_2 using CFM-RP and -0.2 V vs. Ag/AgCl using CFM-RP-Nafion®.

To demonstrate the selectivity of CFM-RP and CFM-RP-Nafion® sensors against the main interferents found in brain tissue, amperometry was performed and the response to H_2O_2 (10 µM addition) was compared to that of dopamine, DOPAC, norepinephrine, 5-hydroxitryptamine, uric acid (5 µM each) and ascorbate (100 µM). As observed in Fig. S4B, no response was detected for the biogenic amines, DOPAC and uric acid.

Both CFM-RP and CFM-RP-Nafion® were calibrated by amperometry to determine the sensitivity, linearity and limit of detection towards H_2O_2. As shown in Fig. 5E and 5F, both sensor types showed good linearity in the concentration range of 2 – 450 µM. Sensitivity, linearity and LOD calculated for the concentration interval of 2-10 µM H_2O_2 are summarized in Table 1 and highlight the adequate analytical properties of both types of sensor for detection of low H_2O_2 concentrations in the brain extracellular space.

Table 1 – Analytical parameters for H_2O_2 reduction obtained at CFM-RP and CFM-RP-Nafion® sensors from calibrations performed in PBS with 4.5 mM K^+ pH 7.4.

	CFM-RP (N=10)	**CFM-RP-Nafion® (N=7)**
Applied *E* (V vs. Ag/AgCl)	-0.1	-0.2
Sensitivity / EAS ($\mu A\ \mu M^{-1}\ cm^{-2}$)	0.98 ± 0.37	0.69 ± 0.12
Linearity (R^2)	0.996 ± 0.006	0.998 ± 0.002
LOD (nM)	70 ± 40	33 ± 16

In the literature one can find other examples of microelectrode-based H_2O_2 sensors. The main analytical properties and applications are summarized in Table 2. It can be seen that the limit of detection is lower than most of the sensors in the literature and with a comparable linear range. Nearly all of the sensors measure H_2O_2 at a significantly positive potential of at least +0.4 V vs. Ag/AgCl which makes them more subject to interferences from other electroactive species. As an alternative to electrochemical techniques, one of the most commonly used methods to quantify extracellular H_2O_2 is based on the ability of heme peroxidases, such as horseradish peroxidase, to catalyze the H_2O_2-dependent oxidation of a tracer compound measured, for example, by a decrease in its fluorescence [47,48]. The major limitations associated with this method include the fact that a number of biological reductants can act as alternative substrates for peroxidases, the presence of fluorescence quenchers in tissues and cells and the ability of the mitochondrial electron chain to reduce the oxidation products [47]. Several methods are available for the quantification of intracellular H_2O_2, as reviewed in [47,48].

Table 2 – Analytical parameters of different microelectrode-based H_2O_2 sensors

Electrode Type	Surface Modification	Applied Potential (V vs. Ag/AgCl)	Sensitivity (mean +/- SD)	LOD (nM)	LR (µM)	Application	[REF]
CFM (ø 33 µm)	RP thin film RP-Nafion®	-0.1 -0.2	0.98 ± 0.37 A M^{-1} cm^{-2} 0.69 ± 0.12 A M^{-1} cm^{-2}	70 33	0-450	*Ex vivo* study in brain slices	This Study
CFM (ø 7 µm)	Mixed iron-ruthenium hexa-cyanoferrate (FeRuHCF) thin film	-0.02	0.66 A M^{-1} cm^{-2}	900	5-1000	*In vitro* evaluation	[49]
CFM (ø 7 µm)	PB combined with PPD	0 vs. SCE	0.45 ± 0.02 A M^{-1} cm^{-2}	100	nd	GOx biosensor design, tested *in vivo* in rodent brain	[50]
CFM (ø 7 µm)	No modification	FSCV	nd	1900	0-2000	*In vivo* study in rodent brain; *Ex vivo* study in brain slices	[8,51]
CFM (ø 7 µm)	PPD	FSCV	0.2 nA $µM^{-1}$	nd	nd	*In vivo* study in rodent brain; *Ex vivo* study in brain slices	[7]
CFM (ø 10 µm)	HRP in a redox polymer containing pendant, non-diffusing, osmium-centered polypyridyl complex	-0.1	7.1 ± 3.2 pA $µM^{-1}$	285	0-10	*In vivo* study in rodent brain	[52]
CFM (ø 10 µm)	Pt_{ED}	0.6	80 nA mM^{-1}	10	1-1000	Single Human Fibroblast	[53]
CFM (ø 33 µm)	Pt_{ED} Nanoparticles/PPD	0.7	2.2 A M^{-1} cm^{-2} (+PPD: 0.66 A M^{-1} cm^{-2})	11	nd	GOx biosensor design, tested in rodent brain slice	[4]
CFM (ø 30 µm)	Ru_{ED}/PPD	0.4	91.5 nA mM^{-1}	500	0.5 - 5	GOx. Lox and GluOx biosensor design, tested in vivo in rodent brain	[54]
CFM (ø 7 µm)	Ti- Cr- Pt_{VD} Nanofilm (100nm)	0.5	1.9 ± 0.7 A M^{-1} cm^{-2} (+PPD: 0.6 A M^{-1} cm^{-2})	10 (+PPD)	nd	LOx and GOx biosensor design, *in vivo* rodent brain	[55]
CNT Fiber (ø ca. 5 µm)	Pd Nanoparticles	-0.5	2.75 A M^{-1} cm^{-2}	2000	2 - 1300	*In vitro* evaluation	[56]
Pt wire (ø 10 µm)	No modification	0.65	224 +/- 20 fA $µM^{-1}$	500	0.5 - 1000	Single Human Monocyte	[57]
Pt wire (ø 25 µm)	No modification	CV (I*p* = -0.8 V vs. AgQRCE)	nd	nd	1000-12000	*Aspergillus fumigatus* mycelium clump	[58]
Pt wire (ø 25 µm)	Pt−MWCNTs−ionic liquid	0.5	2.4 ± 0.24 A M^{-1} cm^{-2}	250	0.25 – 7000	*Streptococcus gordonii* in simulated biofilm	[59]
Pt/Ir, 90%/10% (ø 125 µm)	Nafion/PPD/Catalase/ Glutaraldehyde	0.7	0.45 ± 0.08 nA $µM^{-1}$ (*)	nd	nd	*In vitro* evaluation	[60]
Au wire (ø 25 µm)	Pt_{ED} Nanoparticles (on NPG)	-0.2	75 pA nM^{-1}	0.3	nd	Evaluation in Human breast cancer cells (MCF-7)	[61]
Au wire (ø 50 µm)	Ruthenium Purple/Sol-Gel	-0.05	nd	nd	nd	ATP and Hypoxanthine biosensor design	[21]

CFM - Carbon Fiber Microelectrode; RP – Ruthenium purple; PB – Prussian Blue; PPD – polyphenylenediamine ED - Electrodeposition; FSCV – Fast Scanning Cyclic Voltammetry; HRP - Horseradish peroxidase; GOx – Glucose oxidase; Lox – Lactate oxidase; GluOx – glutamate oxidase; CNT – Carbon Nanotube; NPG – Nanoporous gold; QRCE – Quasi reference counter electrode. * subtracted from blank sensor

3.6. Monitoring Exogenous H_2O_2 in Striatal Slices

To validate that CFM-RP are suitable to measure H_2O_2 concentration dynamics in brain tissue, we performed amperometric recording in rat striatal slices upon local application of a solution of H_2O_2. For this purpose, an array was constructed comprised of a bare CFM and a CFM-RP with an inter-tip distance of 50-100 µm. This array was submerged in the slice recording chamber and perfused with aCSF at 32 ºC. The response towards H_2O_2 was evaluated under these recording conditions by sequential perfusion of H_2O_2 solutions in aCFS with increasing concentrations. As shown in Fig. 6A, the CFM showed good performance under these conditions, while the CFM showed, as expected, no change in current when bathed in H_2O_2.

Following calibration, both were submerged into the tissue using a micromanipulator to guarantee that the whole of the exposed tip was in the tissue core. A micropipette with a tip of 30 µm was position in the center of the two CFM and a small volume of H_2O_2 solution was injected into the tissue. As can be observed in Fig. 5B, this resulted in a transient increase in the reduction current measured at the CFM-RP which was not detected at the bare CFM.

4. Conclusions

In the present study, we have designed and evaluated the analytical performance of a novel CFM modified with RP for monitoring H_2O_2 concentration dynamics in the brain tissue extracellular space. The electrodeposition process used produced a thin film of RP which displayed electrocatalytic behavior for the reduction of H_2O_2 at -0.1V vs. Ag/AgCl in aqueous media with physiological pH 7.4 and a $[Na^+]/[K^+]$ = 30 (total cation concentration of 158 mM), as expected to be found in the brain interstitial fluid. The CFM-RP sensor displayed a linear response over 2 orders of concentration range (2-500 µM), high sensitivity compared to other microelectrode-based sensors for H_2O_2 and a low limit of detection (<100 nM). Furthermore, the improved operational stability under conditions of constant applied potential (-0.2 V vs. Ag/AgCl) afforded by the Nafion® layer combined with the pH stability of the RP as compared to other hexacyanoferrates allows monitoring of H_2O_2 in tissue preparations at physiological pH for up to 3 hours. The suitability of this novel design was demonstrated by measurement of exogenously applied H_2O_2 in rodent striatal brain slices with high spatial and temporal resolution.

Acknowledgements

This work was financed by the European Regional Development Fund (ERDF) through the COMPETE 2020 - Operational Programme for Competitiveness and Internationalization and Portuguese national funds via FCT – Fundação para a Ciência e a Tecnologia, under projects POCI-01-0145-FEDER-028261, UIDB/04539/2020 and UID/EMS/00285/2020.

References

[1] B. Halliwell, M.V. Clement, L.H. Long, Hydrogen peroxide in the human body, FEBS Lett. 486 (2000) 10–13. https://doi.org/10.1016/S0014-5793(00)02197-9.

[2] M.E. Rice, H2O2: A dynamic neuromodulator, Neuroscientist. 17 (2011) 389–406. https://doi.org/10.1177/1073858411404531.

[3] L.J. Murphy, Reduction of Interference Response at a Hydrogen Peroxide Detecting Electrode Using Electropolymerized Films of Substituted Naphthalenes, Anal. Chem. 70 (1998) 2928–2935. https://doi.org/10.1021/ac971182r.

[4] C.F. Lourenço, M. Caetano, A. Ledo, R.M. Barbosa, Platinized carbon fiber-based glucose microbiosensor designed for metabolic studies in brain slices, Bioelectrochemistry. 130 (2019) 107325. https://doi.org/10.1016/j.bioelechem.2019.06.010.

[5] C.A. Cordeiro, M.G. De Vries, T.I.F.H. Cremers, B.H.C. Westerink, The role of surface availability in membrane-induced selectivity for amperometric enzyme-based biosensors, Sensors Actuators, B Chem. 223 (2016) 679–688. https://doi.org/10.1016/j.snb.2015.09.029.

[6] J.P. Lowry, R.D. O'Neill, Homogeneous mechanism of ascorbic acid interference in hydrogen peroxide detection at enzyme-modified electrodes, Anal. Chem. 64 (1992) 453–456. https://doi.org/10.1021/ac00028a022.

[7] L.R. Wilson, S. Panda, A.C. Schmidt, L.A. Sombers, Selective and Mechanically Robust Sensors for Electrochemical Measurements of Real-Time Hydrogen Peroxide Dynamics In Vivo, Anal. Chem. 90 (2017) acs.analchem.7b03770. https://doi.org/10.1021/acs.analchem.7b03770.

[8] A.L. Sanford, S.W. Morton, K.L. Whitehouse, H.M. Oara, L.Z. Lugo-Morales, J.G. Roberts, L.A. Sombers, Voltammetric Detection of Hydrogen Peroxide at Carbon Fiber Microelectrodes, Anal. Chem. 82 (2010) 5205–5210. https://doi.org/10.1021/ac100536s.

[9] C.H. Reid, N.J. Finnerty, Real-time amperometric recording of extracellular H2O2 in the brain of immunocompromised mice: An in vitro, ex vivo and in vivo characterisation study, Sensors (Switzerland). 17 (2017). https://doi.org/10.3390/s17071596.

[10] A.A. Karyakin, O. V. Gitelmacher, E.E. Karyakina, A high-sensitive glucose amperometric biosensor based on prussian blue modified electrodes, Anal. Lett. 27 (1994) 2861–2869. https://doi.org/10.1080/00032719408000297.

[11] A.A. Karyakin, O. V. Gitelmacher, E.E. Karyakina, Prussian Blue-Based First-Generation Biosensor. A Sensitive Amperometric Electrode for Glucose, Anal. Chem. 67 (1995) 2419–2423. https://doi.org/10.1021/ac00110a016.

[12] A.A. Karyakin, Advances of Prussian blue and its analogues in (bio)sensors, Curr. Opin. Electrochem. 5 (2017) 92–98. https://doi.org/10.1016/j.coelec.2017.07.006.

[13] K. Itaya, N. Shoji, I. Uchida, Catalysis of the Reduction of Molecular Oxygen to

Water at Prussian Blue Modified Electrodes, J. Am. Chem. Soc. 106 (1984) 3423–3429. https://doi.org/10.1021/ja00324a007.

[14] F. Ricci, G. Palleschi, Sensor and biosensor preparation, optimisation and applications of Prussian Blue modified electrodes, Biosens. Bioelectron. 21 (2005) 389–407. https://doi.org/10.1016/j.bios.2004.12.001.

[15] B.J. Feldman, R.W. Murray, Electron diffusion in wet and dry Prussian blue films on interdigitated array electrodes, Inorg. Chem. 26 (1987) 1702–1708. https://doi.org/10.1021/ic00258a014.

[16] T. Abe, G. Toda, A. Tajiri, M. Kaneko, Electrochemistry of ferric ruthenocyanide (ruthenium purple), and its electrocatalysis for proton reduction, J. Electroanal. Chem. 510 (2001) 35–42. https://doi.org/10.1016/S0022-0728(01)00539-3.

[17] M.H. Pournaghi-Azar, H. Razmi-Nerbin, Electroless preparation and electrochemistry of nickel-pentacyanonitrosylferrate film modified aluminum electrode, Electroanalysis. (2000). https://doi.org/10.1002/(SICI)1521-4109(200002)12:3<209::AID-ELAN209>3.0.CO;2-I.

[18] R. Garjonyte, A. Malinauskas, Electrocatalytic reactions of hydrogen peroxide at carbon paste electrodes modified by some metal hexacyanoferrates, Sensors Actuators, B Chem. B46 (1998) 236–241. https://doi.org/10.1016/s0925-4005(98)00123-3.

[19] C.G. Tsiafoulis, P.N. Trikalitis, M.I. Prodromidis, Synthesis, characterization and performance of vanadium hexacyanoferrate as electrocatalyst of H2O2, Electrochem. Commun. 7 (2005) 1398–1404. https://doi.org/10.1016/j.elecom.2005.10.001.

[20] K. Itaya, T. Ataka, S. Toshima, Electrochemical Preparation of a Prussian Blue Analogue: Iron-Ruthenium Cyanide, J. Am. Chem. Soc. 104 (1982) 3751–3752. https://doi.org/10.1021/ja00377a048.

[21] F. Tian, E. Llaudet, N. Dale, Ruthenium purple-mediated microelectrode biosensors based on sol-gel film, Anal. Chem. 79 (2007) 6760–6766. https://doi.org/10.1021/ac070822f.

[22] R.M. Santos, C.F. Lourenço, A.P. Piedade, R. Andrews, F. Pomerleau, P. Huettl, G.A. Gerhardt, J. Laranjinha, R.M. Barbosa, A comparative study of carbon fiber-based microelectrodes for the measurement of nitric oxide in brain tissue, Biosens. Bioelectron. 24 (2008) 704–709. https://doi.org/10.1016/j.bios.2008.06.034.

[23] R.J. Mortimer, T.S. Varley, Synthesis, characterisation and in situ colorimetry of electrochromic Ruthenium purple thin films, Dye. Pigment. 89 (2011) 169–176. https://doi.org/10.1016/j.dyepig.2010.10.009.

[24] T.R.I. Cataldi, G.E. De Benedetto, C. Campa, Electrochemical quartz crystal microbalance study and electrochromic behavior of a novel ruthenium purple film, J. Electroanal. Chem. 437 (1997) 93–98. https://doi.org/10.1016/S0022-0728(97)00117-4.

[25] J. Mocak, A.M. Bond, S. Mitchell, G. Scollary, A statistical overview of standard

(IUPAC and ACS) and new procedures for determining the limits of detection and quantification: Application to voltammetric and stripping techniques (Technical Report), Pure Appl. Chem. 69 (1997) 297–328. https://doi.org/10.1351/pac199769020297.

[26] C.E. Banks, R.G. Compton, A.C. Fisher, I.E. Henley, The transport limited currents at insonated electrodes, Phys. Chem. Chem. Phys. 6 (2004) 3147. https://doi.org/10.1039/b403751k.

[27] C.F. Chen, C.M. Wang, Ruthenium purple-containing zeolite modified electrodes and their application for the detection of glucose, J. Electroanal. Chem. 466 (1999) 82–89. https://doi.org/10.1016/S0022-0728(99)00129-1.

[28] K.P. Rajan, V.D. Neff, Electrochromism In the Mixed-Valence Hexacyanides. 2. Kinetics of the Reduction, J. Phys. Chem. 804 (1982) 4361–4368.

[29] S.M. Chen, S.H. Hsueh, Iron Hexacyanoruthenate Films and Their Electrocatalytic Properties with Nitrite and Dopamine, J. Electrochem. Soc. 150 (2003). https://doi.org/10.1149/1.1604113.

[30] K. Sone, M. Yagi, Spectrocyclic voltammetry of Ruthenium purple electrodeposited on a WO 3/tris(2,2'-bipyridine)-ruthenium(II)/polymer hybrid film, Macromol. Symp. 235 (2006) 179–186. https://doi.org/10.1002/masy.200650321.

[31] A. Roos, W.F. Boron, Intracellular pH., Physiol. Rev. 61 (1981) 296–434. https://doi.org/10.1152/physrev.1981.61.2.296.

[32] A.P. Brown, F.C. Anson, Cyclic and Differential Pulse Voltammetric Behavior of Reactants Confined to the Electrode Surface, Anal. Chem. 49 (1977) 1589–1595. https://doi.org/10.1021/ac50019a033.

[33] S.C. Shyu, C.M. Wang, Characterizations of iron-containing clay modified electrodes and their applications for glucose sensing, J. Electrochem. Soc. 145 (1998) 154–158. https://doi.org/10.1149/1.1838228.

[34] T.R.I. Cataldi, G.E. De Benedetto, On the ability of ruthenium to stabilize polynuclear hexacyanometallate film electrodes, J. Electroanal. Chem. (1998). https://doi.org/10.1016/S0022-0728(98)00327-1.

[35] P. Salazar, M. Martín, R.D. O'Neill, R. Roche, J.L. González-Mora, Surfactant-promoted Prussian Blue-modified carbon electrodes: Enhancement of electro-deposition step, stabilization, electrochemical properties and application to lactate microbiosensors for the neurosciences, Colloids Surfaces B Biointerfaces. 92 (2012) 180–189. https://doi.org/10.1016/j.colsurfb.2011.11.047.

[36] E. Laviron, General expression of the linear potential sweep voltammogram in the case of diffusionless electrochemical systems, J. Electroanal. Chem. 101 (1979) 19–28. https://doi.org/10.1016/S0022-0728(79)80075-3.

[37] R. Guidelli, R.G. Compton, J.M. Feliu, E. Gileadi, J. Lipkowski, W. Schmickler, S. Trasatti, IUPAC Technical Report Defining the transfer coefficient in electrochemistry: An assessment (IUPAC Technical Report) 1, (2014). https://doi.org/10.1515/pac-2014-5026.

[38] K. Itaya, H. Akahoshi, S. Toshima, Electrochemistry of Prussian Blue Modified Electrodes: An Electrochemical Preparation Method, J. Electrochem. Soc. 129 (1982) 1498–1500. https://doi.org/10.1149/1.2124191.

[39] P. Salazar, M. Martín, R.D. O'Neill, R. Roche, J.L. González-Mora, Improvement and characterization of surfactant-modified Prussian blue screen-printed carbon electrodes for selective H2O2 detection at low applied potentials, J. Electroanal. Chem. 674 (2012) 48–56. https://doi.org/10.1016/j.jelechem.2012.04.005.

[40] S. Husmann, A.J.G. Zarbin, Multifunctional carbon nanotubes/ruthenium purple thin films: Preparation, characterization and study of application as sensors and electrochromic materials, Dalt. Trans. 44 (2015) 5985–5995. https://doi.org/10.1039/c4dt02784a.

[41] S. Husmann, E. Nossol, A.J.G. Zarbin, Carbon nanotube/Prussian blue paste electrodes: Characterization and study of key parameters for application as sensors for determination of low concentration of hydrogen peroxide, Sensors Actuators, B Chem. 192 (2014) 782–790. https://doi.org/10.1016/j.snb.2013.10.074.

[42] A. Schmidt, S. Husmann, A.J.G. Zarbin, Carbon nanotube thin films modified with a mixture of Prussian blue and ruthenium purple: combining materials and properties, J. Solid State Electrochem. 22 (2018) 2003–2012. https://doi.org/10.1007/s10008-018-3899-x.

[43] J.J. García-Jareño, J. Navarro-Laboulais, F. Vicente, Electrochemical study of nafion membranes/prussian blue films on ito electrodes, Electrochim. Acta. 41 (1996) 2675–2682. https://doi.org/10.1016/0013-4686(96)00121-1.

[44] A. Ledo, C.F. Lourenço, J. Laranjinha, G.A. Gerhardt, R.M. Barbosa, Combined in vivo Amperometric Oximetry and Electrophysiology in a Single Sensor – a Tool for Epilepsy Research, Anal. Chem. 89 (2017) acs.analchem.7b03452. https://doi.org/10.1021/acs.analchem.7b03452.

[45] N.R. Ferreira, A. Ledo, J. Laranjinha, G.A. Gerhardt, R.M. Barbosa, Simultaneous measurements of ascorbate and glutamate in vivo in the rat brain using carbon fiber nanocomposite sensors and microbiosensor arrays, Bioelectrochemistry. 121 (2018) 142–150. https://doi.org/10.1016/j.bioelechem.2018.01.009.

[46] M. Miele, M. Fillenz, In vivo determination of extracellular brain ascorbate, J. Neurosci. Methods. (1996). https://doi.org/10.1016/S0165-0270(96)00094-5.

[47] M.B. Grisham, Methods to detect hydrogen peroxide in living cells: Possibilities and pitfalls, Comp. Biochem. Physiol. - A Mol. Integr. Physiol. 165 (2013) 429–438. https://doi.org/10.1016/j.cbpa.2013.02.003.

[48] A. Boveris, E. Martino, A.O.M. Stoppani, Evaluation of the horseradish peroxidase-scopoletin method for the measurement of hydrogen peroxide formation in biological systems, Anal. Biochem. 80 (1977) 145–158. https://doi.org/10.1016/0003-2697(77)90634-0.

[49] R. Pauliukaite, S.B.B. Hočevar, E.A.A. Hutton, B. Ogorevc, Novel electrochemical microsensor for hydrogen peroxide based on iron-ruthenium hexacyanoferrate modified carbon fiber electrode, Electroanalysis. 20 (2008) 47–53.

https://doi.org/10.1002/elan.200704047.

[50] P. Salazar, M. Martín, R. Roche, R.D. O'Neill, J.L. González-Mora, Prussian Blue-modified microelectrodes for selective transduction in enzyme-based amperometric microbiosensors for in vivo neurochemical monitoring, Electrochim. Acta. 55 (2010) 6476–6484. https://doi.org/10.1016/j.electacta.2010.06.036.

[51] M. Spanos, J. Gras-Najjar, J.M. Letchworth, A.L. Sanford, J.V. Toups, L.A. Sombers, Quantitation of hydrogen peroxide fluctuations and their modulation of dopamine dynamics in the rat dorsal striatum using fast-scan cyclic voltammetry, ACS Chem. Neurosci. 4 (2013) 782–789. https://doi.org/10.1021/cn4000499.

[52] N. V. Kulagina, A.C. Michael, Monitoring hydrogen peroxide in the extracellular space of the brain with amperometric microsensors, Anal. Chem. 75 (2003) 4875–4881. https://doi.org/10.1021/ac034573g.

[53] S. Arbault, P. Pantano, J.A. Jankowski, M. Vuillaume, C. Amatore, Monitoring an oxidative stress mechanism at a single human fibroblast, Anal. Chem. 67 (1995) 3382–3390. https://doi.org/10.1021/ac00115a004.

[54] O.M. Schuvailo, O.O. Soldatkin, A. Lefebvre, R. Cespuglio, A.P. Soldatkin, Highly selective microbiosensors for in vivo measurement of glucose, lactate and glutamate, Anal. Chim. Acta. 573–574 (2006) 110–116. https://doi.org/10.1016/j.aca.2006.03.034.

[55] C. Chatard, A. Sabac, L. Moreno-Velasquez, A. Meiller, S. Marinesco, Minimally Invasive Microelectrode Biosensors Based on Platinized Carbon Fibers for in Vivo Brain Monitoring, ACS Cent. Sci. 4 (2018) 1751–1760. https://doi.org/10.1021/acscentsci.8b00797.

[56] Y. Liu, G. Sun, C. Jiang, X.T. Zheng, L. Zheng, C.M. Li, Highly sensitive detection of hydrogen peroxide at a carbon nanotube fiber microelectrode coated with palladium nanoparticles, Microchim. Acta. 181 (2014) 63–70. https://doi.org/10.1007/s00604-013-1066-8.

[57] M. Bozem, P. Knapp, V. Mirčeski, E.J. Slowik, I. Bogeski, R. Kappl, C. Heinemann, M. Hoth, Electrochemical Quantification of Extracellular Local H 2 O 2 Kinetics Originating from Single Cells, Antioxid. Redox Signal. 29 (2018) 501–517. https://doi.org/10.1089/ars.2016.6840.

[58] C.S. Santos, R. Bannitz-Fernandes, A.S. Lima, C.A. Tairum, I. Malavazi, L.E.S. Netto, M. Bertotti, Monitoring H 2 O 2 inside Aspergillus fumigatus with an Integrated Microelectrode: The Role of Peroxiredoxin Protein Prx1, Anal. Chem. 90 (2018) 2587–2593. https://doi.org/10.1021/acs.analchem.7b04074.

[59] V.S. Joshi, J. Kreth, D. Koley, Pt-Decorated MWCNTs-Ionic Liquid Composite-Based Hydrogen Peroxide Sensor to Study Microbial Metabolism Using Scanning Electrochemical Microscopy, Anal. Chem. 89 (2017) 7709–7718. https://doi.org/10.1021/acs.analchem.7b01677.

[60] K.B. O'Brien, S.J.J. Killoran, R.D. O'Neill, J.P.P. Lowry, K.B. O'Brien, S.J.J. Killoran, R.D. O'Neill, J.P.P. Lowry, Development and characterization in vitro of a

catalase-based biosensor for hydrogen peroxide monitoring, Biosens. Bioelectron. 22 (2007) 2994–3000. https://www.sciencedirect.com/science/article/pii/S0956566306006129 (accessed April 10, 2018).

[61] C. Xiao, Y.L. Liu, J.Q. Xu, S.W. Lv, S. Guo, W.H. Huang, Real-time monitoring of H2O2 release from single cells using nanoporous gold microelectrodes decorated with platinum nanoparticles, Analyst. 140 (2015) 3753–3758. https://doi.org/10.1039/c4an02056a.

Figure Legends

Figure 1 – A) Electrodeposition of RP on the surface of CFM by cyclic voltammetry at 50 mV s^{-1} showing the 1st (black) and 10th (blue) scan followed by stabilization of the RP film by CV in a $RuCl_3$ solution (red). B) Profile of the RP film in phosphate buffer 10 mM, pH 7.4, with different K^+/Na^+ ratios. Cyclic voltammetry was performed at 10 mV s^{-1}.

Figure 2 – Scanning Electron Micrographs of the bare CFM (A) and CFM-RP (B and C) surface; EDS elemental analysis of the CFM/RP surface (D).

Figure 3 – A) Cyclic voltammograms of RP deposited on the surface of a CFM at different scan rates (0.01 to 5 V s^{-1}) in 0.1 M KCl + 0.01 M HCl. B) Dependence of both anodic and cathodic peak currents on scan rate, which is linear for v <0.3 V s^{-1} (inset). C) Linear dependence of anodic and cathodic peak potentials on the square root of scan rate for v > 0.3 V s^{-1}. D) Dependence of oxidation and reduction potential on log (v / V s^{-1}).

Figure 4 – A) Stability of the thin film RP on the CFM surface derived from repeated voltammograms in 0.1 M KCl + HCl 0.01 M (black) and in PBS with 4.5 mM K^+ pH 7.4. B) Evaluation of stability of the RP film over an extended 3 h period in PBS + 4.5 mM K^+, pH 7.4 under conditions of open circuit between CV scans for CFM-RP (purple) and CFM-PB (blue) and when the potential is held at -0.1V vs. Ag/AgCl between successive scans for CFM-RP (black) and for CFM-RP-Nafion® (red). In panel B, error bars are shown only in one direction for the sake of graphical clarity.

Figure 5 – Linear sweep voltammograms for CFM-RP (A) and CFM-RP-Nafion® (B) sensors obtained in PBS with 4.5 mM K^+, pH 7.4 and for increasing amounts of H_2O_2. Fixed-potential amperometric response for CFM-RP (C) and CFM-RP-Nafion® (D) towards H_2O_2 (black), ascorbate (red) and O_2 (blue). Calibration of CFM-RP at -0.1 V vs. Ag/AgCl (E) and CFM-RP-Nafion® -0.2 V vs. Ag/AgCl (F) between 2-450 µM H_2O_2 in PBS

with 4.5 mM K^+ pH 7.4. Highlighted in the gray box is the section between 2-10 µM H_2O_2 and the insets in the lower right corner show the linear regression for each calibration. In panels C and D, error bars are shown only in one direction for the sake of graphical clarity.

Figure 6 – Monitoring Exogenously Applied H_2O_2 in Striatal Slices. A) Calibration of an array comprised of a CFM-RP (red) and bare CFM (black) (tip distance 100 µm) in the slice perfusion chamber, at 32 ºC, in aCFS. Inset is the corresponding calibration curve. B) Recording of amperometric current at CFM-RP/CFM array inserted into tissue core upon repetitive application of a 1mM H_2O_2 solution through a micropipette (30 µm tip diameter) placed between the two CFM. Inset is a magnification of one of the signals.

Figure 1

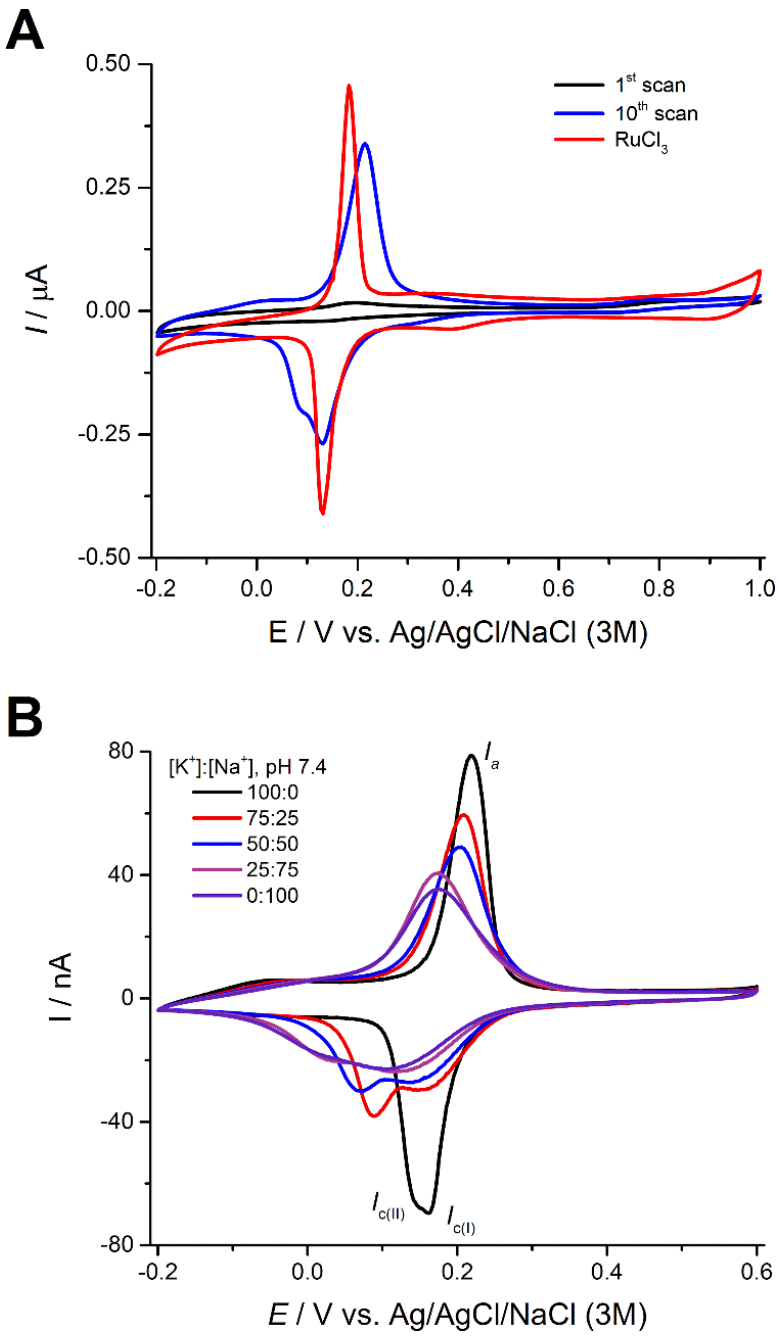
A
0.50
0.25
0.00
-0.25
-0.50
I / µA
1st scan
10th scan
RuCl3
-0.2
0.0
0.2
0.4
0.6
0.8
1.0
E / V vs. Ag/AgCl/NaCl (3M)
B
80
40
0
-40
-80
I / nA
[K+]:[Na+], pH 7.4
100:0
75:25
50:50
25:75
0:100
Ia
Ic(II)
Ic(I)
-0.2
0.0
0.2
0.4
0.6
E / V vs. Ag/AgCl/NaCl (3M)

Figure 2

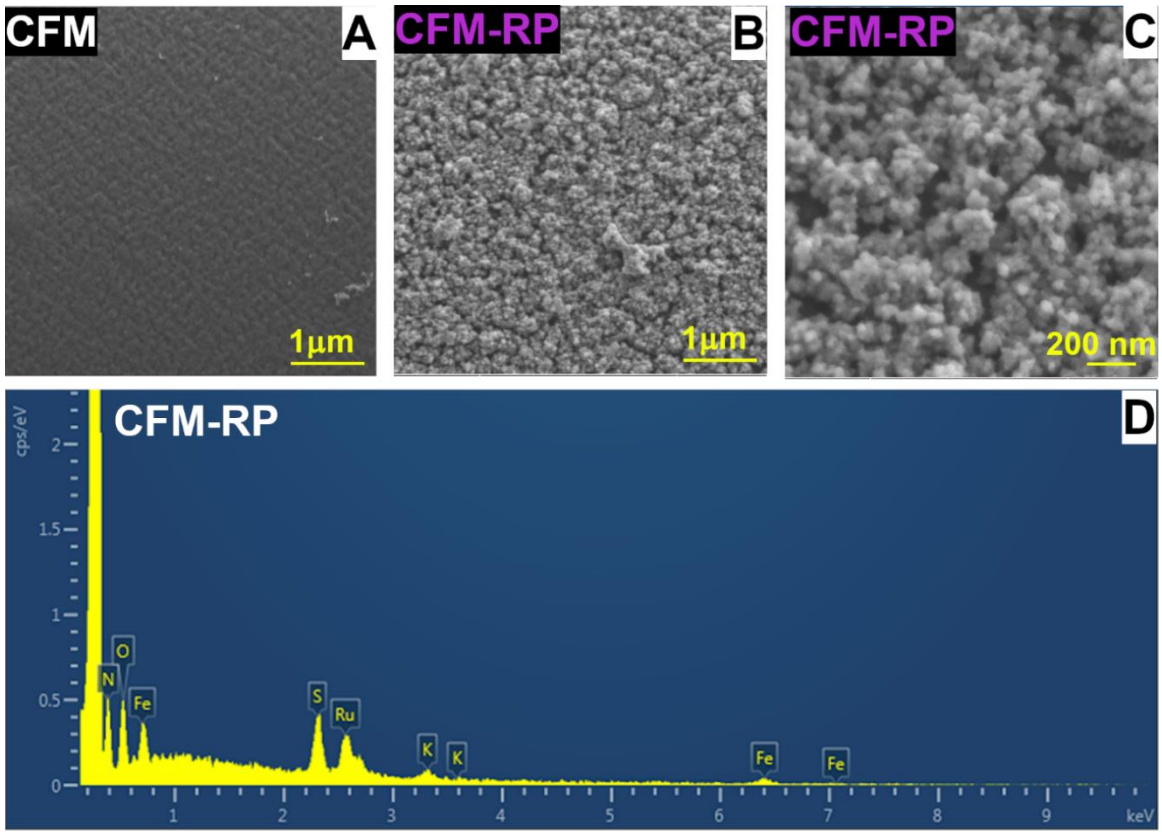
CFM
A
1µm
CFM-RP
B
1µm
CFM-RP
C
200 nm
CFM-RP
D
cps/eV
O
N
Fe
S
Ru
K
K
Fe
Fe
keV

Figure 3

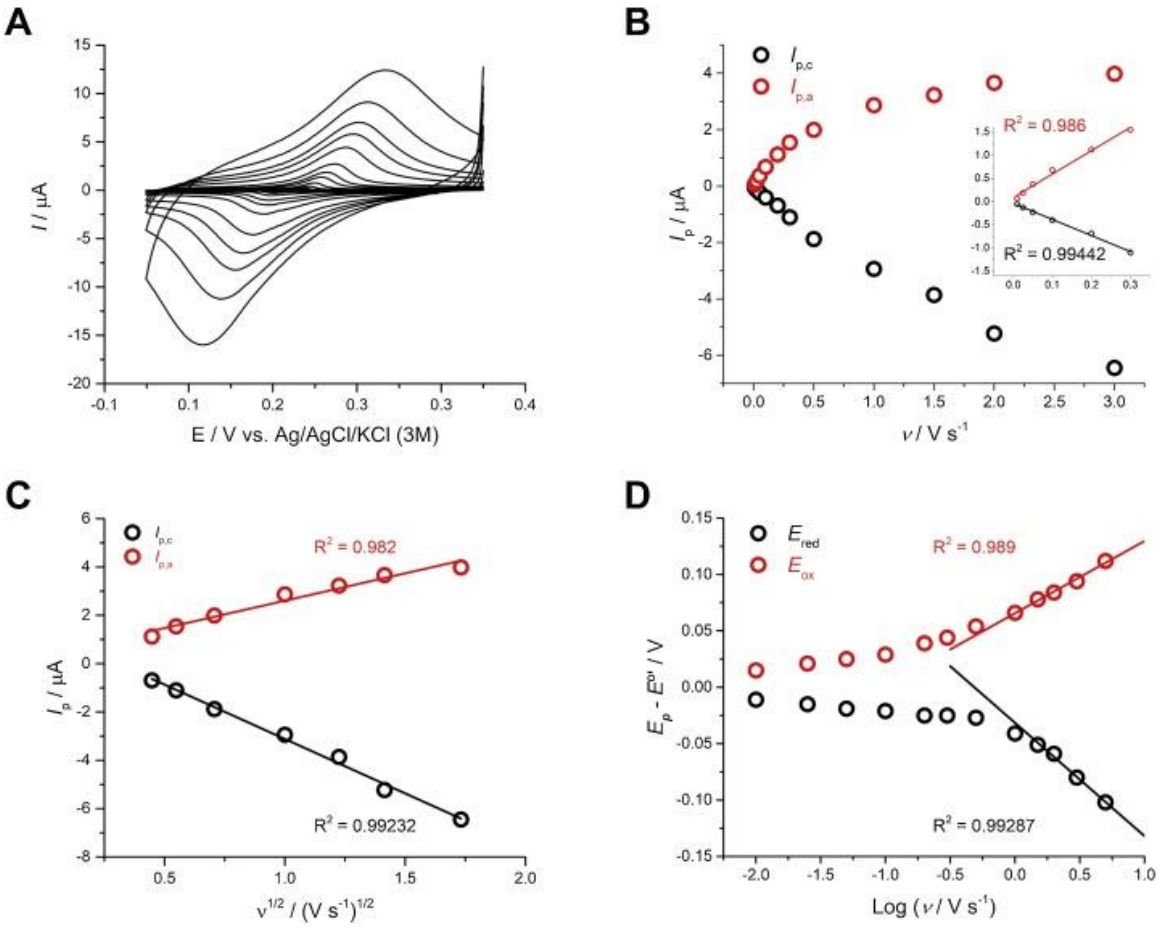
A
I / µA
E / V vs. Ag/AgCl/KCl (3M)
B
$I_{p,c}$
$I_{p,a}$
I_p / µA
ν / V s^{-1}
R^2 = 0.986
R^2 = 0.99442
C
$I_{p,c}$
$I_{p,a}$
R^2 = 0.982
R^2 = 0.99232
I_p / µA
$\nu^{1/2}$ / (V s^{-1})$^{1/2}$
D
E_{red}
E_{ox}
R^2 = 0.989
R^2 = 0.99287
E_p - $E^{o'}$ / V
Log (ν / V s^{-1})

Figure 4

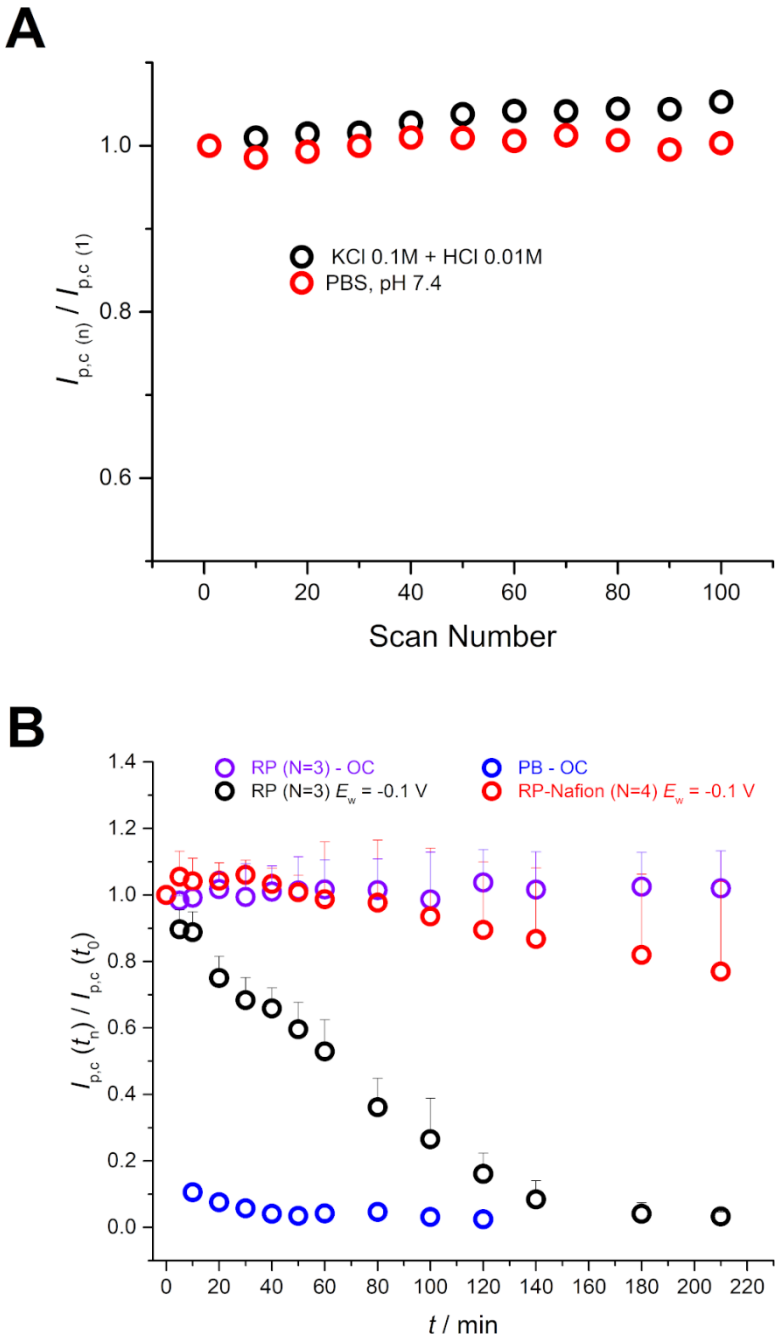
A
1.0
0.8
0.6
$I_{p,c\ (n)}$ / $I_{p,c\ (1)}$
KCl 0.1M + HCl 0.01M
PBS, pH 7.4
0
20
40
60
80
100
Scan Number
B
RP (N=3) - OC
RP (N=3) E_w = -0.1 V
PB - OC
RP-Nafion (N=4) E_w = -0.1 V
1.4
1.2
1.0
0.8
0.6
0.4
0.2
0.0
$I_{p,c}$ (t_n) / $I_{p,c}$ (t_0)
0
20
40
60
80
100
120
140
160
180
200
220
t / min

1 Figure 5

2

3

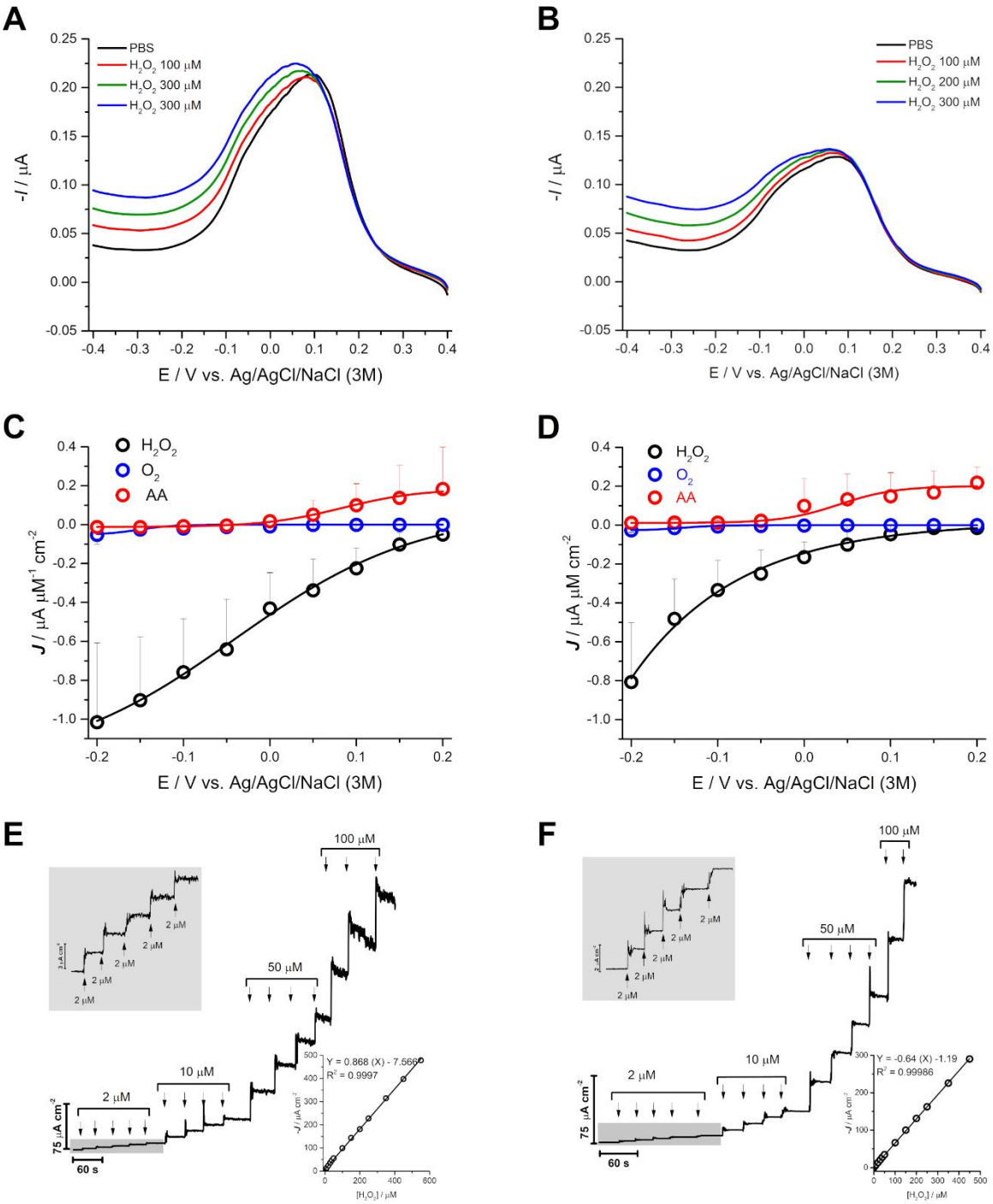

4

5

6

1 Figure 6

2

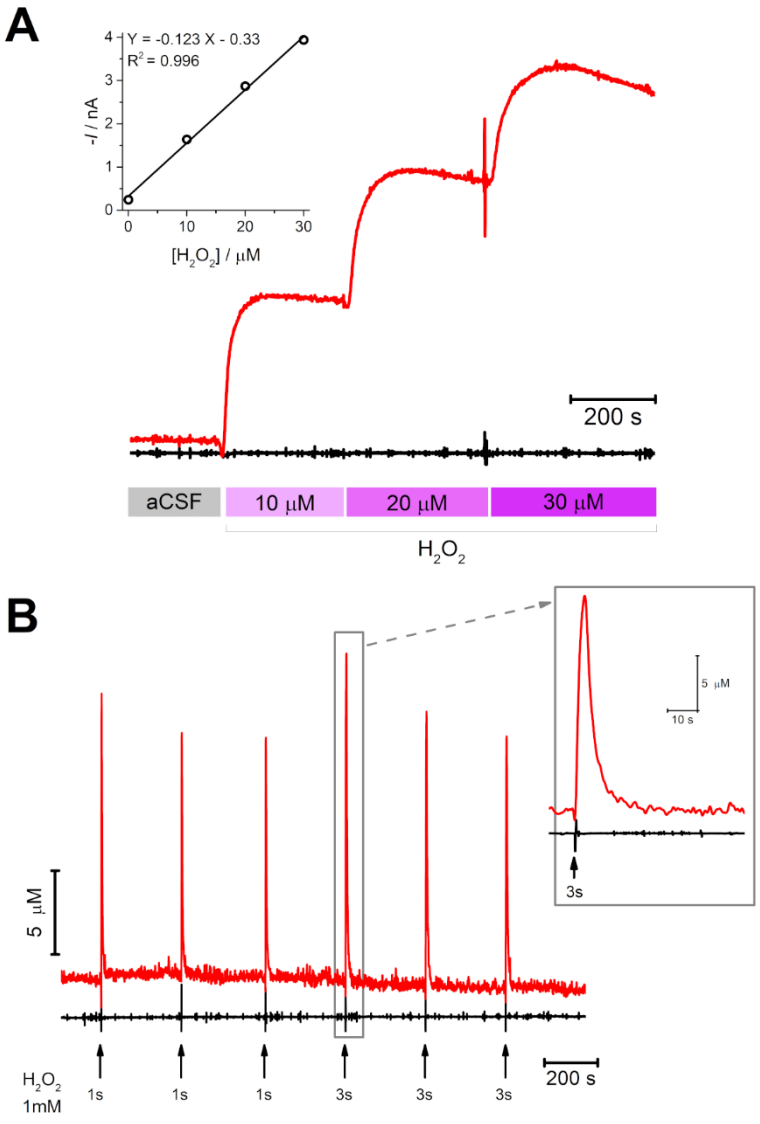
A
Y = -0.123 X - 0.33
R² = 0.996
-I / nA
[H2O2] / µM
200 s
aCSF
10 µM
20 µM
30 µM
H2O2
B
5 µM
10 s
3s
5 µM
H2O2
1mM
1s
1s
1s
3s
3s
3s
200 s